Effect of entrance-channel parameters on incomplete fusion reactions

Abhishek Yadav,[1,*] Vijay R. Sharma,[1] Pushpendra P. Singh,[2,†] Devendra P. Singh,[1] R. Kumar,[3] Unnati,[1] M. K. Sharma,[4] B. P. Singh,[1] R. Prasad,[1] and R. K. Bhowmik[3]

[1]*Department of Physics, Aligarh Muslim University, Aligarh (U.P.) 202 002, India*

[2]*Institute for Nuclear Physics, Technical University Darmstadt, Schlossgartenstrasse 9, D-64289 Darmstadt, Germany*

[3]*NP-Group, Inter-University Accelerator Center, New Delhi 110067, India*

[4]*Department of Physics, Shri Varshney College, Aligarh (U.P.), India*

(Received 4 May 2012; revised manuscript received 28 May 2012; published 25 June 2012)

In order to disentangle the contribution of complete and incomplete fusion components and to study their dependence on various entrance-channel observables, the measurement and analysis of forward recoil ranges, which is the direct measure of linear momentum transfer from projectile to the target nuclei, has been done in the interaction of ^{12}C beam with ^{159}Tb target nucleus at three distinct above-barrier energies ≈74, 80, and 87 MeV. The recoil-catcher technique followed by off-line γ-ray spectroscopy has been used. The complete and incomplete fusion events have been tagged by full and partial linear momentum transfer components, respectively. The observed incomplete fusion events have been explained on the basis of the breakup fusion model where these events may be attributed to the fusion of ^{8}Be and/or ^{4}He from ^{12}C projectile to the target nucleus. Analysis of the data indicates that the incomplete fusion has significant contribution at the studied energies and its contribution has been found to increase with the beam energy. An attempt has also been made to understand the projectile structure effect on the underlying reaction dynamics.

DOI: 10.1103/PhysRevC.85.064617 PACS number(s): 25.60.Dz, 25.70.Gh, 25.70.Jj

I. INTRODUCTION

The interest to study the incomplete fusion (ICF) reactions at energies ≈4–7 MeV/nucleon has increased recently due to the observation of these reactions at such low energies, where complete fusion (CF) is expected to be the sole contributor to the total fusion cross section [1–10]. In the case of CF, the projectiles for $\ell < \ell_{\rm crit}$ merge with the target nucleus, with the dominance of the nuclear force field, leading to the formation of a completely fused excited composite system. However, in the case of ICF, for ℓ values $>\ell_{\rm crit}$, the projectile may break up into clusters, and one of the clusters may fuse with the target nucleus, forming the reduced excited composite system with relatively less mass, charge, and excitation energy compared to the completely fused composite system. The remnant flows in the forward direction with almost beam velocity. Due to this partial fusion of the projectile, the fractional momentum transfer takes place in the ICF processes. Each of these processes (CF and ICF) leads to the characteristic velocity distribution of the reaction residues. As such, the distribution of measured yields of the residues as a function of velocity and/or the ranges in a stopping medium may give an insight into the reaction mechanism involved. Though the differences in the velocity and ranges of CF and ICF reaction products are not so significant, by using very thin catcher foils (≈μg/cm^2), it is possible to separate the CF and ICF residues. The breakup of heavy-ion projectiles may also be understood on the basis of disappearance of the fusion pocket in the one-dimensional effective potential energy curve, as the angular momentum (ℓ) increases beyond the critical limit ($\ell_{\rm crit}$) of complete fusion. In order to provide sustainable input angular momentum and/or to restore the fusion pocket in the potential energy curve, the projectile may break up into clusters and a part fuses with the target nucleus, while the other may escape and carries away the excess angular momentum. As such, there is a deficit in the linear momentum of composite system, compared to the total linear momentum [11–16]. It may be pointed out that there are conflicting reports on the dependence of ICF on the angular momenta. The γ-multiplicity measurements done by Inamura *et al.* [17], Wilczynski *et al.* [18], Gerschel *et al.* [19], and Trautmann *et al.* [20] showed that ICF involves $\ell \geqslant \ell_{\rm crit}$. However, studies [21] on spherical targets showed involvement of ℓ values in ICF lower than $\ell_{\rm crit}$ for CF. This suggests that ICF competes with CF even at $\ell \leqslant \ell_{\rm crit}$, contrary to the hypothesis of the SUMRULE model [22,23] of ICF. Parker *et al.* [4] observed forward peaked α particles in reactions of ^{12}C on ^{51}V at $E \approx 6$ MeV/nucleon. Morgenstern *et al.* [24] measured the velocity spectra of evaporation residues (ERs) in reactions of ^{12}C, ^{20,22}Ne beams of energies ≈10–25 MeV/nucleon with ^{40,44,48}Ca, ^{58,60,62}Ni targets, where the deviation in velocity spectra from the mean velocity of complete fusion has been observed, indicating the incomplete momentum (mass) transfer from projectile to the target nucleus. Tserruya *et al.* [21] found the evidence for ICF from time-of-flight (TOF) measurements of ERs in the reactions of ≈5.5–10 MeV/nucleon ^{12}C with ^{120}Sn, ^{160}Gd, and ^{197}Au. In one of our recent letters [25] it has also been shown that the ICF reactions may originate during the peripheral interactions.

The breakup fusion model [26,27], hot spot model [28], SUMRULE model [22,23], promptly emitted particles [29], and exciton model [30,31] etc., are some of the models generally used to describe such reactions. These models are found to fit the experimental data at projectile energies, $E_{\rm lab} \geqslant 10$ MeV/nucleon to a large extent. However, the onset

*abhishekyadav117@gmail.com
†pushpendrapsingh@gmail.com

 ©2012 American Physical Society

of ICF from just near to well above the Coulomb barrier energies observed recently triggered a resurgent interest in the study of ICF dynamics at low energies [32–37]. However, some of the most debated and outstanding issues related to low-energy ICF have been, (i) the energy dependence of ICF processes, (ii) the localization of the ℓ window, (iii) the usefulness of ICF to populate high-spin states in final reaction products, and (iv) the effect of entrance-channel parameters on the onset and strength of ICF. In recent years, high-quality experimental data on cross sections [9], spin distributions (SDs) of residues [25], and linear momentum distributions [16] of reaction products have been obtained at the Inter-University Accelerator Center (IUAC), New Delhi. These studies concluded that the ICF contributes at low energies, but is limited only to a few projectile-target combinations. The measurement of forward recoil range distributions (FRRDs) can be used as one of the irrefutable methods to distinguish the different ICF components, where the same residue may be formed by more than one fusion channel. In the present work, in order to facilitate the experimental disentanglement of these competing processes (CF and ICF), the FRRDs of reaction residues populated in ^{12}C + ^{159}Tb interactions at three beam energies ≈74, 80, and 87 MeV have been measured. In the present work, an attempt has also been made to have quantitative information of ICF reactions. The present work is in continuation of our recent investigation on the same system ^{12}C + ^{159}Tb, where the measurement and analysis of excitation functions have been used to investigate the role of breakup processes [35,36]. The present paper is organized as follows. A brief description of the experimental setup is given in Sec. II, while Sec. III deals with the details of the measurements and analysis of RRDs, and finally the conclusion is presented in Sec. IV.

II. EXPERIMENTAL DETAILS

The experiments have been performed using ^{12}C ion beam delivered from the 15UD-Pelletron accelerator at the Inter-University Accelerator Center (IUAC), New Delhi, India. Although the experimental methodology is similar to that in our earlier work [16,33], for quick reference a brief description is given here. In the present work, three different stacks, each consisting of a ^{159}Tb target (abundance = 100%) followed by a series of thin Al-catcher foils (different in each irradiation depending on the energy of the beam), to trap the recoiling residues, have been irradiated separately by the ^{12}C beams of ≈74, 80, and 87 MeV energy. The targets were prepared by the rolling method, while, the thin Al-catcher foils were made by vacuum evaporation technique. The thickness of each sample and catcher foil has been measured by the α-transmission method. The thickness of the target was ≈190 μg/cm^2, however, the thicknesses of Al catchers ranged from ≈15–50 μg/cm^2. The samples were pasted on rectangular Al holders (size ≈2.5 × 2.1 cm^2) having concentric holes of 10 mm diameter. The irradiations have been performed in the general purpose scattering chamber (GPSC) having an invacuum transfer facility (ITF). A stack of the thin Al-catcher foils (sufficient to stop the compound nucleus (CN) formed via full linear momentum transfer) was placed just after the target, so that the heavy recoiling residues populated via CF and/or ICF could be trapped at their respective ranges in Al-catcher foil thicknesses. The irradiations have been carried out for ≈12 h, with a beam current ≈4pnA. The total charge collected in the Faraday cup has been used to obtain the beam flux during the irradiations. The activities produced in each Al-catcher foil have been recorded separately using a precalibrated high-resolution HPGe spectrometer of 100 c.c. active volume coupled to the CAMAC-based CANDLE [38] software. The resolution of the γ spectrometer was ≈2 keV, for 1.33 MeV γ ray of ^{60}Co source. The geometry-dependent efficiency of the HPGe detector for various γ-ray energies at different source-detector separations was determined using the standard ^{152}Eu source. The identification of populated reaction products have been made on the basis of their characteristic γ-ray energies, and has been further confirmed by measuring their half-lives as well. A list of identified reaction residues populated in ^{12}C + ^{159}Tb interactions are tabulated in Table I, along with their spectroscopic properties [39,40]. The present technique of measuring cross sections has been found to work well in the mass region of interest with well established level schemes where the γ lines are well separated for different residues.

TABLE I. List of identified reaction residues (channels) with their spectroscopic properties.

Residue	$T_{1/2}$	J^π	E_γ(keV)	I^γ (%)
^{168}Lu^{g+m} (3n)	5.5 min	3$^+$	198.86	180.0[a]
			228.58	70.0[a]
^{167}Lu (4n)	51.5 min	7/2$^+$	213.21	3.5
^{165}Lu (6n)	10.74 min	1/2$^+$	120.58	25
			360.51	8.2
^{167}Yb (p3n)	17.5 min	5/2$^-$	176.2	20.4
			177.26	2.7
^{165}Tm (α2n)	30.06 h	1/2$^+$	242.85	35
			346.75	3.9
			356.44	3.7
			460.12	3.7
^{163}Tm(α4n)	1.81 h	1/2$^+$	190.07	1.28
			239.67	4.1
			471.29	3.8
^{161}Ho(2α2n)	2.48 h	7/2$^-$	103.03	3.6
^{160}Ho^g(2α3n)	25.6 min	5$^+$	645.25	16.20
^{160}Ho^m(2α3n)	5.02 h	2$^-$	645.25	16.20
			728.18	30.8
			879.39	20.2

[a]These intensities are relative.

III. ANALYSIS AND INTERPRETATION OF RESULTS

As has been mentioned earlier, the measurement of the projected ranges of the reaction products gives the degree of linear momentum transfer ($\rho_{\rm LMT}$) from the projectile to the target nucleus and thus is an irrefutable method to disentangle the CF and/or ICF reactions. The velocity distribution of a given type of reaction products is symmetric about $v_\circ$, having a width that depends upon the evaporation process and, in particular, on the particles evaporated from CN. The mean

velocity $v_\circ$, may be given as

$$v_\circ = v_{CN} = \frac{\sqrt{2M_P E}}{M_{P+T}}, \quad (1)$$

where M_P is the projectile mass, M_{P+T} is the total mass of the composite system (projectile+target), and E is the projectile energy. Thus, the degree of linear momentum transfer may be given as

$$\rho_{\rm LMT} = \frac{P_{\rm frac}}{P_{\rm proj}}, \quad (2)$$

where, $P_{\rm frac}$ is the linear momentum of the fused fraction of the projectile and $P_{\rm proj}$ is the entire linear momentum of the projectile. As already mentioned, $\rho_{\rm LMT}$ is proportional to the fused mass of the projectile (i.e., maximum LMT may give maximum recoil velocity to the reaction products). This is a promising way of investigating the full momentum transfer in the case of the complete-fusion process, and relatively small momentum transfer in a partial momentum transfer reaction (ICF). Since, in the CF process, the maximum $\rho_{\rm LMT}$ is transferred from the projectile to the target nucleus, therefore, for a given entrance channel the CN has predetermined mass, energy, and momenta. While, in the case of ICF, a partial $\rho_{\rm LMT}$ results due to the formation of an incompletely fused composite system in the excited state. For an incompletely fused composite system, the mass, energy, and momenta of CN may not have unique values. This may be because of the fluctuations in the fused mass from the projectile to target nucleus and various interaction trajectories. Thus, the experimentally measured forward recoil ranges of final reaction products in the stopping medium gives information about the $\rho_{\rm LMT}$ involved.

As already mentioned, the identification of the trapped recoiling reaction products in the catcher foils was made by their characteristic γ radiations as well as by measuring their half-lives. The production cross sections ($\sigma_{\rm ER}$) for identified reaction products were computed using the standard formulation given in Ref. [32]. In order to obtain the normalized yields as a function of cumulative depth in the Al stopping medium, the cross section of the reaction products in each catcher foil was divided by its thickness. The resulting normalized yields have been plotted against cumulative catcher foil thicknesses to obtain the recoil range distributions for the identified residues viz., ^{168}Lu ($3n$), ^{167}Lu ($4n$), ^{165}Lu ($6n$), ^{167}Yb ($p3n$), ^{165}Tm ($\alpha 2n$), ^{163}Tm ($\alpha 4n$), ^{161}Ho ($2\alpha 2n$), ^{160}Ho^g ($2\alpha 3n$), and ^{160}Ho^m ($2\alpha 3n$). As a representative case, to show CF and ICF components, the RRDs for ^{167}Lu ($4n$), ^{165}Tm ($\alpha 4n$), and ^{161}Ho ($2\alpha 2n$) residues have been presented in Figs. 1–3, at three different beam energies ≈74, 80, and 87 MeV. In the recoil range measurements, the cross sections for the production of a given residue as a function of the range are affected by relative errors, which depend essentially only on the counting statistics and the uncertainty in the catcher thicknesses and in presently studied cases, are less than or, at most, around 15%. The size of the circles in Figs. 1–3, includes the uncertainty in the yield values. The measured FRRDs clearly indicate the different momentum transfer components, depending on the fused mass of the projectile with the target nucleus. In case of the $4n$ channel (Fig. 1), the measured RRDs show only a single peak at all the three bombarding energies,

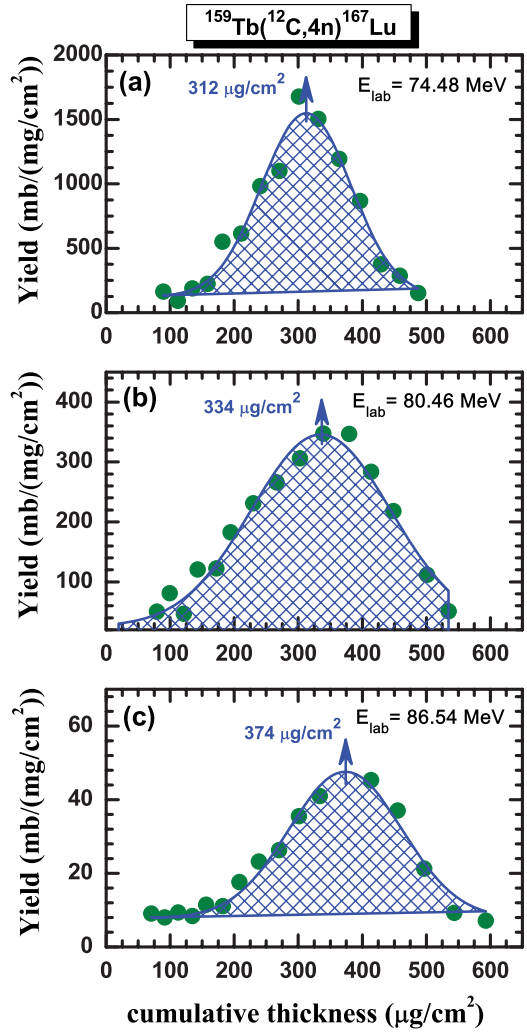

FIG. 1. (Color online) Measured FRRDs for ^{167}Lu residues populated via $4n$ channel at ≈74, 80, and 87 MeV beam energies.

indicating only one linear momentum transfer component (a characteristic of the CF process) involved in the production of ^{167}Lu residues. A close observation of the range distribution of ^{167}Lu residues (Fig. 1) reveals that the FRRD peak shifts toward relatively higher cumulative catcher thickness with increase in beam energy. Further, it may be pointed out that, the neutron emission from the forward recoiling residues may change their energy and momentum of the final residue, depending on the direction of emission. This is reflected in the width (FWHM) of the experimentally measured recoil range distributions. The width may also arise because of the contributions from straggling. The identified reaction products and their experimentally measured most probable ranges, $R_p^{\rm expt}$ in Al, in units of μg/cm^2, for all the CF residues along with the theoretically estimated (using the code SRIM [41]) mean ranges $R_p^{\rm theo}$ in Al, in units of μg/cm^2, are given in Table II. The most probable recoil ranges ($R_p^{\rm theo}$) have been calculated, assuming that in the case of CF, the incoming ion completely fuses with the target nucleus and transfers its total linear momentum to the fused system, which recoils for the conservation of

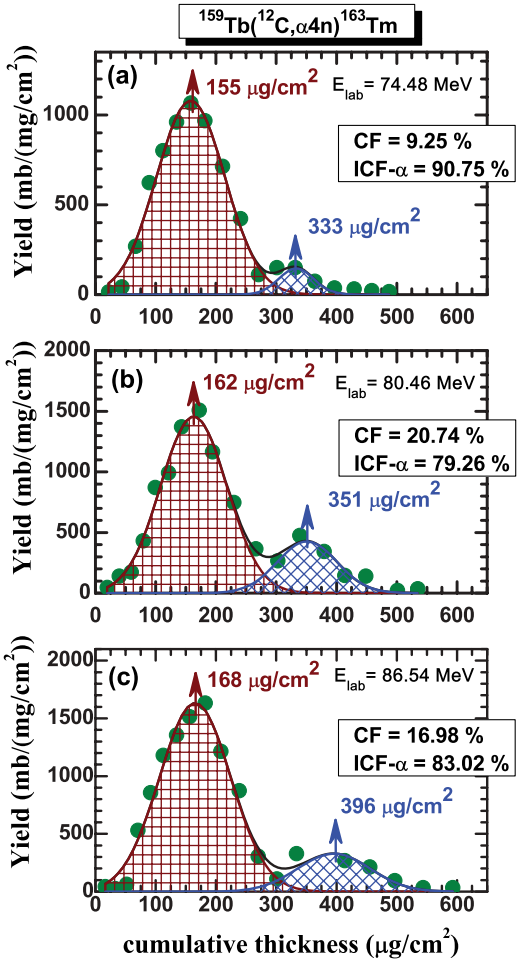

FIG. 2. (Color online) Typical FRRDs for ^{165}Tm populated via $\alpha 2n$ channel at ≈74, 80, and 87 MeV beam energies, having two Gaussian peaks in range distributions.

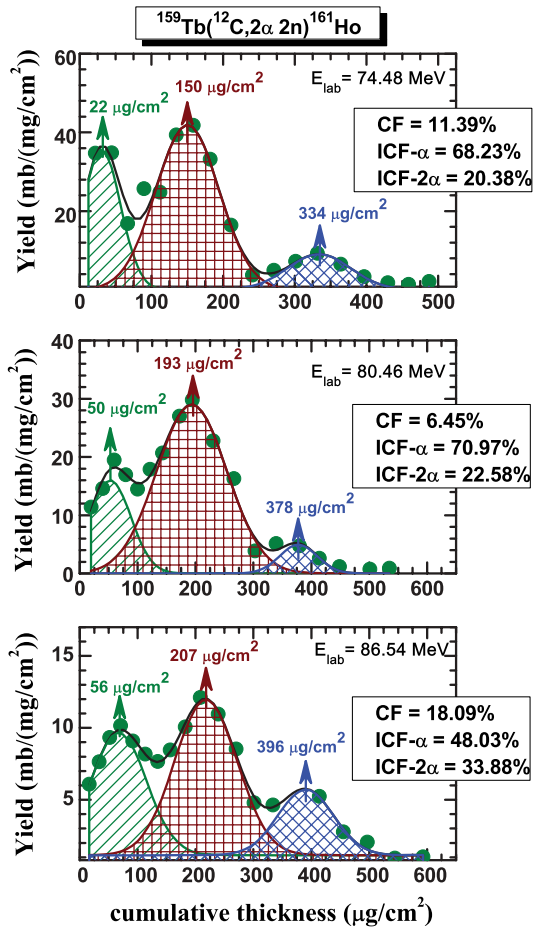

FIG. 3. (Color online) Measured FRRDs for ^{161}Ho residues populated via $2\alpha 2n$ channel at ≈74, 80, and 87 MeV beam energies, having three different momentum transfer components.

linear momentum. An attempt has also been made to check the consistency in the FWHM of the observed FRRDs. The normalized FWHM (FWHM/R_p^{expt}) has been deduced for the observed distributions and tabulated in Table III. The normalized FWHM has been found to be consistence for the CF and ICF residues individually. As can be seen from Table III that for α-emitting channels, the average peak resolution for CF is ≈0.28, while for ICF-α and ICF-2α the average peak resolution increases to ≈0.69 and 1.78, respectively, as expected. On the basis of the previous description, it is clear that the population of reaction products ^{167}Lu produced via 4n channel is associated with the entire LMT from projectile to the target nucleus, and may be represented as

$$^{12}\mathrm{C} + {}^{159}\mathrm{Tb} \Rightarrow {}^{171}\mathrm{Lu}^{*} \Rightarrow {}^{167}\mathrm{Lu} + 4n$$

In a similar way, the FRRDs for the residues ^{168}Lu (3n), ^{165}Lu (6n), and ^{167}Yb ($p3n$) are found to have a single peak associated with complete linear momentum transfer from projectile to the composite nucleus, indicating the production of these residues via the CF process only.

Further, in case of α-emitting channels, the residues ^{165}Tm, ^{163}Tm, ^{161}Ho, ^{160}Ho^g, and ^{160}Ho^m are expected to be populated, respectively via $\alpha 2n$, $\alpha 4n$, $2\alpha 2n$, and $2\alpha 3n$ channels. The observed FRRDs were resolved into two Gaussian peaks, for αxn channels, using the ORIGIN software. As a representative case, the FRRDs for the residues, ^{163}Tm ($\alpha 4n$), have been plotted at three different energies in Figs. 2(a)–2(c). As can be seen from Fig. 1, the FRRDs may be fitted

TABLE II. Experimentally measured most probable ranges $R_{p(\mathrm{exp})}$ deduced from RRD curves, and theoretically calculated forward mean ranges $R_{p(\mathrm{the})}$, in Al in units of μg/cm^2 for CF and ICF components using the range energy relation along with the reaction products produced in the interaction of ^{12}C with ^{159}Tb at ≈74 MeV.

Residues	$R^{CF}_{p(\mathrm{exp})}$	$R^{CF}_{p(\mathrm{the})}$	$R^{ICF-^8Be}_{p(\mathrm{exp})}$	$R^{ICF-^8Be}_{p(\mathrm{the})}$	$R^{ICF-^4He}_{p(\mathrm{exp})}$	$R^{ICF-^4He}_{p(\mathrm{the})}$
^{168}Lu	315 ± 43	321	-	-	-	-
^{167}Lu	312 ± 48	321	-	-	-	-
^{165}Lu	314 ± 52	321	-	-	-	-
^{167}Yb	330 ± 28	321	-	-	-	-
^{165}Tm	340 ± 32	321	163 ± 23	150	-	-
^{163}Tm	333 ± 61	321	158 ± 19	150	-	-
^{161}Ho	334 ± 53	321	150 ± 21	150	22 ± 8	21
^{160}Ho^g	348 ± 32	321	141 ± 28	150	23 ± 9	21
^{160}Ho^m	337 ± 61	321	145 ± 26	150	25 ± 11	21

TABLE III. Comparison of normalized FWHM of the distributions.

Residues	≈74 MeV CF	≈80 MeV CF	≈87 MeV CF	≈74 MeV ICF-α	≈80 MeV ICF-α	≈87 MeV ICF-α	≈74 MeV ICF-2α	≈80 MeV ICF-2α	≈87 MeV ICF-2α
^{168}Lu ($3n$)	0.62	0.77	-	-	-	-	-	-	-
^{167}Lu ($4n$)	0.56	0.70	0.65	-	-	-	-	-	-
^{165}Lu ($6n$)	0.67	0.65	0.67	-	-	-	-	-	-
^{167}Yb ($p3n$)	0.58	0.63	0.71	-	-	-	-	-	-
^{165}Tm ($\alpha 2n$)	0.31	0.25	0.22	0.83	0.72	0.81	-	-	-
^{163}Tm ($\alpha 4n$)	0.20	0.30	0.34	0.87	0.80	0.83	-	-	-
^{161}Ho ($2\alpha 2n$)	0.32	0.20	0.34	0.69	0.75	0.63	1.89	1.66	1.80
^{160}Ho ($2\alpha 3n$)	0.27	0.22	0.26	0.74	0.79	0.73	1.81	1.76	1.90

with two Gaussian peaks, one at ≈333 ± 32, 351 ± 60, and 396 ± 65 μg/cm^2 in Al for three beam energies, indicating the complete momentum transfer events, however, another peak at lower cumulative depth at ≈155 ± 23, 162 ± 40, and 168 ± 45 μg/cm^2 corresponds to the fusion of ^{8}Be (if ^{12}C is assumed to break up into ^{8}Be + α and ^{8}Be fuses) with ^{159}Tb target nucleus. Similarly, the FRRDs for other αxn channels have been resolved into two Gaussian peaks, indicating the presence of more than one linear momentum transfer components. It is observed that the complete as well as the incomplete momentum transfer peaks in the range spectra are centered at the expected position shown by the arrow. It may be observed from Fig. 2 that the mean range R_p^{expt} shifts towards higher cumulative catcher thickness as the beam energy increases, as expected. It may be inferred that the residues ^{163}Tm populated through $\alpha 4n$ channel may be populated via two ways

(i) Fusion of ^{12}C

$$^{12}\mathrm{C} + {}^{159}\mathrm{Tb} \Rightarrow {}^{171}\mathrm{Lu}^* \Rightarrow {}^{163}\mathrm{Tm} + \alpha 4n \quad \text{and/or} \quad 2p6n$$

or

(ii) Fusion of ^{8}Be (α as spectator)

$$\begin{aligned} {}^{12}\mathrm{C}({}^{8}\mathrm{Be} + \alpha) &\Rightarrow {}^{8}\mathrm{Be} + {}^{159}\mathrm{Tb} \\ &\Rightarrow {}^{167}\mathrm{Tm}^* + \alpha \quad \text{(as spectator)} \\ &\Rightarrow {}^{167}\mathrm{Tm}^* \Rightarrow {}^{163}\mathrm{Tm} + 4n. \end{aligned}$$

Further, in case of $2\alpha xn$ channels, the measured FRRDs have been found to be resolved into three Gaussian peaks. The measured FRRDs for $2\alpha 2n$ channel have been plotted in Figs. 3(a)–3(c) at three beam energies. In this figure the observation of three peaks may be understood assuming the breakup of ^{12}C into possible α clusters. The peaks at ≈334 ± 53, 378 ± 47, and 396 ± 67 μg/cm^2 depths for three beam energies are attributed to the complete momentum transfer (i.e., fusion of ^{12}C with the target nucleus). However, the peaks at ≈150 ± 21, 193 ± 37, and 207 ± 29 μg/cm^2 for three beam energies belongs to the partial linear momentum transfer ($\frac{2}{3}\rho_{\mathrm{LMT}}^{\mathrm{CF}}$) (i.e., the fusion of ^{8}Be). Another peak at the lowest cumulative depth corresponds to the fusion of the α particle with the target nucleus, involving $\frac{1}{3}\rho_{\mathrm{LMT}}^{\mathrm{CF}}$. As such, it can be inferred that the residues ^{161}Ho produced through $2\alpha 2n$ channel have the contribution from both the processes, namely, CF as well as ICF, which may be represented as

(i) Fusion of ^{12}C

$$^{12}\mathrm{C} + {}^{159}\mathrm{Tb} \Rightarrow {}^{171}\mathrm{Lu}^* \Rightarrow {}^{161}\mathrm{Ho} + 2\alpha 2n \quad \text{and/or} \quad 4p6n,$$

(ii) Fusion of ^{8}Be (α as spectator)

$$\begin{aligned} {}^{12}\mathrm{C}({}^{8}\mathrm{Be} + \alpha) &\Rightarrow {}^{8}\mathrm{Be} + {}^{159}\mathrm{Tb} \\ &\Rightarrow {}^{167}\mathrm{Tm}^* + \alpha \quad \text{(as spectator)} \\ &\Rightarrow {}^{167}\mathrm{Tm}^* \Rightarrow {}^{161}\mathrm{Ho} + \alpha 2n, \end{aligned}$$

or

(iii) Fusion of α (^{8}Be as spectator)

$$\begin{aligned} {}^{12}\mathrm{C}({}^{8}\mathrm{Be} + {}^{4}\mathrm{He}) &\Rightarrow {}^{4}\mathrm{He} + {}^{159}\mathrm{Tb} \\ &\Rightarrow {}^{163}\mathrm{Ho}^* + {}^{8}\mathrm{Be} \quad \text{(as spectator)} \\ &\Rightarrow {}^{163}\mathrm{Ho}^* \Rightarrow {}^{161}\mathrm{Ho} + 2n. \end{aligned}$$

The above description is based on the breakup fusion model, where it is assumed that the incident ^{12}C ion breaks into fragments (e.g., ^{8}Be + α or α + ^{8}Be) as it enters in the nuclear field of the target nucleus. The fragments so produced are assumed to move nearly with the same velocity as that of incident ion. One of the fragments (^{8}Be or α) fuses with the target nucleus forming an incompletely fused composite system, which recoils in the forward direction to conserve the input linear momentum. In order to compare the range-integrated yields of CF and ICF reactions, the statistical model calculations have been done using the code PACE4 [42], which is the upgraded version of code PACE2 [43]. The code PACE2 [43] is a modified version of JULIAN, the Hillman-Eyal evaporation code using a Monte Carlo code coupling angular momentum. The code PACE4 [42] has several new features, including a user friendly Windows interface, where explanation for each parameter is displayed. Further, a database for binding energies is also included in this program. The code PACE4 [42] gives almost similar results except that it is quite user friendly and simple. This code is based on the statistical approach of CN de-excitation by Monte Carlo procedure. In code PACE4 [42] the angular momentum projections are calculated at each step of de-excitation. The angular momentum conservation is explicitly taken into account, and the CF cross sections are calculated using the BASS formula [44]. The partial cross section (σ_ℓ) for the formation of compound nucleus at a particular angular momentum ℓ, and specific bombarding energy, E is given by

$$\sigma_\ell = \frac{\lambda^2}{4\pi}(2\ell + 1)T_\ell, \tag{3}$$

where λ is reduced wavelength. Transmission coefficients T_ℓ may be given by the expression

$$T_\ell = \left[1 + \exp\left(\frac{\ell - \ell_{\max}}{\Delta}\right)\right]^{-1}, \tag{4}$$

TABLE IV. Experimentally measured forward recoil range integrated cross section $\sigma_{\text{exp}}^{\text{RRD}}$ deduced from RRD curves, and theoretically calculated cross-section $\sigma_{\text{theo}}^{\text{PACE}}$ at ≈74, 80, and 87 MeV.

Residues	Energy (E) ≈ 74 MeV		Energy (E) ≈ 80 MeV		Energy (E) ≈ 87 MeV	
	$\sigma_{\text{exp}}^{\text{RRD}}$	$\sigma_{\text{theo}}^{\text{PACE}}$	$\sigma_{\text{exp}}^{\text{RRD}}$	$\sigma_{\text{theo}}^{\text{PACE}}$	$\sigma_{\text{exp}}^{\text{RRD}}$	$\sigma_{\text{theo}}^{\text{PACE}}$
^{168}Lu ($3n$)	3.20	3.18	1.10	0.97	-	-
^{167}Lu ($4n$)	297	314	96	90.2	12.0	15.9
^{165}Lu ($6n$)	1.4	0.61	120	109	510	298
^{167}Yb ($p3n$)	33	29	13.3	12.05	2.82	3.07
^{165}Tm ($\alpha 2n$)	6.79	0.83	11.15	0.28	17.32	0.24
^{163}Tm ($\alpha 4n$)	165.32	10.98	260.9	38.05	280.44	53.09
^{161}Ho ($2\alpha 2n$)	7.27	0.20	5.94	0.23	3.34	0.14

where Δ is the diffuseness parameter, while $\ell_{\max}$ is the maximum amount of ℓ determined by total fusion cross section,

$$\sigma_F = \sum_{\ell=0}^{\infty} \sigma_\ell \tag{5}$$

The optical model potentials of Becchetti and Greenlees [45] have been used for calculating the transmission coefficients for neutron and proton, and for α-particle emission. In the description of γ-ray competitions, emission of E1, E2, M1, and M2 γ rays are included and the γ-ray strength functions for different transitions are taken from tables of Endt [46].

Further, the relative contributions of complete and incomplete fusion in the production of a particular reaction product may be computed by fitting the experimentally measured RRDs with a Gaussian distribution using the ORIGIN software. The Gaussian yield curves of evaporation residues obtained from RRD are given by

$$Y = Y_0 + \frac{A}{\omega_A^2\sqrt{2\pi}} e^{-(R-R_P)^2/2\pi\omega_A^2}, \tag{6}$$

where R_P is the most probable mean range, ω_A is the width parameter (FWHM) of the distribution, and A is the area under the peak. Further, the normalized yield Y may be estimated by the χ square fit (χ^2) of the experimentally determined range distributions and may be represented as follows:

$$\chi^2 = \frac{1}{(m-p-1)}\{Y(A) - Y_0(A)\}^2 \tag{7}$$

The value of the χ square (χ^2) was minimized in this analysis using a nonlinear least-square fit routine, keeping the width parameter (ω_A) and most probable mean range (R_P) in the FRRD as a free parameter. Moreover, as indicated in Figs. 2 and 3, the residues involving α-emitting channels show more than one RRD component. In such cases, the experimentally measured normalized yields have been fitted using the multipeak option in a similar way as mentioned above. The contribution of different fusion components have been obtained by dividing the area under the peak of the corresponding fusion component by the total area associated with the experimental data. It has been observed that the contribution of CF satisfactorily matches with that predicted by PACE4 code with physically reasonable parameters [35,36], which were optimized to reproduce the evaporation residues populated in case of complete fusion reactions such as xn and pxn channels. However, the contribution of ICF reactions (given in Table IV) could not be reproduced by calculations using the same set of parameters since PACE code does not take ICF into account.

A. Dependence on projectile energy

In order to study the energy dependence of CF (full LMT) and ICF (partial LMT) components, percentage relative contributions of the CF and ICF components are deduced using the relation,

$$F_{\text{ICF}} = \frac{\Sigma\sigma_{\text{ICF}}}{\Sigma\sigma_{\text{CF}} + \Sigma\sigma_{\text{ICF}}} \times 10^2, \tag{8}$$

where $\Sigma\sigma_{\text{CF}}$ and $\Sigma\sigma_{\text{ICF}}$ are the complete and incomplete fusion cross sections at the studied energies. The percentage ICF contributions of different fusion components have been obtained by dividing the area under the ICF peak of the corresponding fusion component by the total area associated with the experimental data. The values of F_{ICF} deduced from FRRDs data are also compared with the F_{ICF} obtained from the excitation function measurements [35], as a function of beam

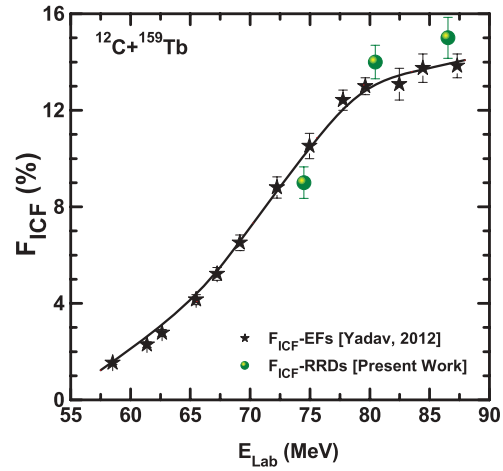

FIG. 4. (Color online) The percentage incomplete fusion fraction (F_{ICF}) deduced from the analysis of forward recoil range distributions as a function of projectile energy. Data shown by black stars are obtained from Yadav's analysis of EFs [35].

TABLE V. Comparison of range integrated cross-section with the cross-sections obtained from EFs measurement for $3n$, $4n$, $6n$ and $p3n$-channels.

Residues	≈74 MeV RRD (EFs)	≈80 MeV RRD (EFs)	≈87 MeV RRD (EFs)
^{168}Lu ($3n$)	3.2 (3.4)	1.1 (0.76)	-
^{167}Lu ($4n$)	297 (320)	96 (90)	12 (10)
^{165}Lu ($6n$)	1.4 (1.05)	120 (124)	510 (550)
^{167}Yb ($p3n$)	33 (32.2)	13.3 (11.6)	2.8 (3.6)

energy ($E_{\rm lab}$) in Fig. 4. As can be seen from this figure, the ICF fraction increases rapidly with energy at lower energies, however, at relatively higher energies the $F_{\rm ICF}$ seems to increase with slow rate. Nevertheless, it may also be observed from Fig. 4, that both the measurements of FRRDs and the EFs give nearly same $F_{\rm ICF}$, which strengthens the present measurements and indicates the self-consistency of the data. In Table V comparison of range-integrated cross sections with the cross sections obtained from EFs measurement for xn and pxn channels has also been done, which matches reasonably. It may not be out of place to mention that similar observations of ICF contributions increasing with energy and mass asymmetry have been obtained by Morgenstern *et al*. [24]. However, their work involved measuring the velocity spectra employing the time-of-flight method in lighter systems and also at relatively higher energies ≈10–25 MeV/nucleon.

B. Comment on mass-asymmetry and projectile structure effect

In order to have better understanding about the dependence of underlying reaction dynamics on mass asymmetry and/or projectile structure, the presently deduced $F_{\rm ICF}$ values have been compared with the $F_{\rm ICF}$ obtained in the ^{16}O induced reactions on same target ^{159}Tb [14]. The Fig. 5, shows the comparison of $F_{\rm ICF}$ for both the systems. It is evident from this figure that the ^{16}O as projectile has higher ICF contribution than for the ^{12}C, at the same normalized projectile energies. But

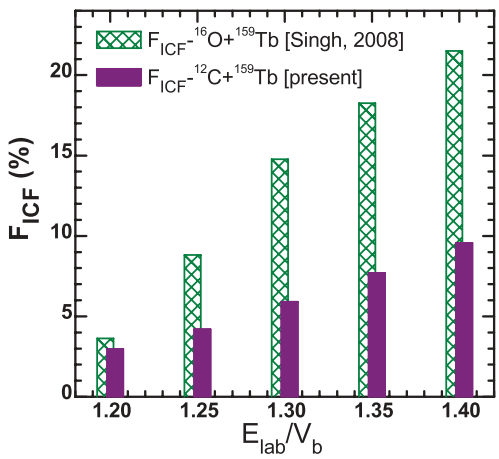

FIG. 5. (Color online) The percentage incomplete fusion fraction ($F_{\rm ICF}$) deduced for ^{16}O + ^{159}Tb from Singh [9] and ^{12}C + ^{159}Tb (present work) as a function of reduced projectile energy.

according to Morgenstern's mass-asymmetry systematics the more asymmetric system would have more ICF probability. The mass asymmetry of interacting partners is defined as $\mu = A_T/(A_T + A_P)$. So ^{12}C + ^{159}Tb ($\mu = 0.9298$) should have more ICF than ^{16}O + ^{159}Tb ($\mu = 0.9086$). However, the binding energy aspect ($E^{^{16}O}_{\rm binding} > E^{^{12}C}_{\rm binding}$) is also unable to explain the present picture. One of the possible explanations may be the excess of α cluster in ^{16}O versus ^{12}C. In addition to this the α-Q value for ^{16}O is less than the ^{12}C (i.e., ^{16}O requires less energy to break up into α clusters than ^{12}C and thus gives large ICF contributions). As such, the α-Q value of the projectile seems to be a reasonable parameter to explain the presently observed large $F_{\rm ICF}$ values for ^{16}O as projectile than for the ^{12}C.

C. SUMRULE calculations: sharp cutoff in ℓ distribution

In the SUMRULE model [22,23], which is based on the partial statistical equilibrium and on the idea of generalized concept of critical angular momentum, the transfer of mass may occur only if the angular momentum of relative motion of the captured fragment P^p (P^p: participant, P^s: spectator) with respect to the target nucleus is smaller than the critical angular momentum for this incompletely fused system (i.e., $\ell_{\rm eff} \leqslant \ell^{P^p+T}_{\rm crit}$). The limiting angular momentum in the reference frame of the entrance channel, $\ell_{\rm limit}$, is related to the critical angular momentum $\ell^{P^p+T}_{\rm crit}$ of fused part as

$$\ell_{\rm limit} = \frac{A_p A_T}{(A_{P^s} A_p + A_{P^p} A_T)} \ell^{P^p+T}_{\rm crit}. \tag{9}$$

However, for a mass-asymmetric projectile-target combination, the limiting angular momentum may be rewritten as

$$\ell_{\rm limit} \sim \frac{A_p}{A_{P^p}} \ell^{P^p+T}_{\rm crit}. \tag{10}$$

By assuming the smooth cutoff in the ℓ space the transmission coefficient for each individual reaction channel is given as

$$T_\ell(i) = \left[1 + \exp\left(\frac{\ell - \ell_{\rm limit}(i)}{\Delta}\right)\right]^{-1}, \tag{11}$$

where Δ gives the diffuseness in the ℓ distribution. For small ℓ values the transmission coefficients T_ℓ are almost unity for all channels. The different reaction channels open up one after the other with increasing angular momentum and depending upon their corresponding limiting angular momenta $\ell_{\rm limit}(i)$, hence the reaction probabilities for a given partial wave ℓ

$$N_\ell \sum_i T_\ell(i) \times \exp\left\{\frac{Q_{gg}(i) - Q_c(i)}{T}\right\} = 1, \tag{12}$$

where N_ℓ is the ℓ-dependent normalization factor common for all reaction channels. Thus, absolute cross sections for the individual reaction channels are defined as

$$\sigma(i) = \pi \lambda\!\!\!^{-2} \sum_{\ell=0}^{\ell_{\rm max}} (2\ell + 1) \times \frac{T_l(i) p(i)}{\sum_j T_l(j) p(j)}, \tag{13}$$

where $\lambda\!\!\!^{-2} = \hbar^2/(2\mu E)$ is the reduced wavelength for the entrance channel and $p(i)$ is the reaction probability for a

given channel i, which is proportional to $\sim\exp[\{Q_{gg}(i) - Q_c(i)\}/T]$, T is an effective temperature, and $Q_c(i)$ is the change of the Coulomb interaction energy due to the transfer of charge. The ℓ_{max} is defined as the largest ℓ for which the colliding system penetrates into the region where the total nucleus-nucleus potential is attractive and/or the distance of closest approach is smaller than the sum of the half-density radii, however, the critical angular momenta ℓ_{crit}, which determine the magnitude of the transmission coefficients T_ℓ, for individual reaction channels were calculated from a simplified formula as

$$\ell_{crit}^2 = \frac{\mu_m (C_1 + C_2)^3}{\hbar^2}\left[4\pi\gamma\frac{C_1 C_2}{C_1 + C_2} - \frac{Z_1 Z_2 e^2}{(C_1 + C_2)^2}\right], \quad (14)$$

where μ_m is the reduced mass of the interacting partners, γ is the surface tension coefficient, Z_1, Z_2 and C_1, C_2 are the atomic numbers and half-density radii of projectile and target nuclei, respectively. With this model one may calculate absolute cross sections for CF, ICF channels, and other binary reactions, which presumably proceed via the formation of a dinuclear system. The model contains three free parameters: the effective temperature T, the effective Coulomb interaction radius R_c, and the diffuseness in ℓ distributions, Δ. Wilczynski *et al.* [22], to fit the experimental data in the ^{14}N + ^{159}Tb reaction at $E_{lab} = 140$ MeV, used $T = 3.5$ MeV, $R_c/(A_P^{1/3} + A_T^{1/3}) = 1.5$, and $\Delta = 1.7\hbar$. In order to obtain the magnitude of the ICF-reaction cross section in the present work, the same parameters have been retained. Using these parameters, the SUMRULE model calculations highly underestimate the measured cross sections for residues of interest. As a typical example the experimentally measured cross sections for the $(\alpha 2n)$ and $(2\alpha 3n)$ channels are $\approx 64.0 \pm 9.6$ mb and 5.0 ± 0.7 mb, however, the theoretically calculated SUMRULE values are 1.32 mb and 0.02 mb at 86 MeV beam energy. These substantial discrepancies indicate the need for refinement in the assumptions of the SUMRULE model. Similar deviations have also been found by Parker *et al.* [4] in their study on the ^{12}C + ^{51}V system up to 100 MeV.

D. Diffuseness in ℓ distribution: Observation of incomplete fusion at $\ell < \ell_{crit}$

In order to have better understanding about the diffuseness in ℓ distribution, the critical angular momentum ℓ_{crit} for the present system at which the pocket in the entrance-channel potential vanishes has been calculated using the prescription of Wilzyanski *et al.* [18]. The calculation gives ℓ_{crit} as $46\hbar$. The fusion ℓ distributions for the compound nucleus in ^{12}C + ^{159}Tb interactions at studied energies, have been calculated using the code CCFULL [47], and are plotted in Fig. 6. The values of ℓ_{max} at three respective energies in the present work are $\approx$36, 40, 44$\hbar$, respectively, which are less than the ℓ_{crit} for fusion for this system. The SUMRULE model assumes sharp cutoff ℓ values for the CF and ICF processes. The underestimation of the ICF cross section by the SUMRULE model may be due to the assumption in the model that a major contribution to the ICF reactions comes from the collision trajectories with the angular momentum ℓ greater than the

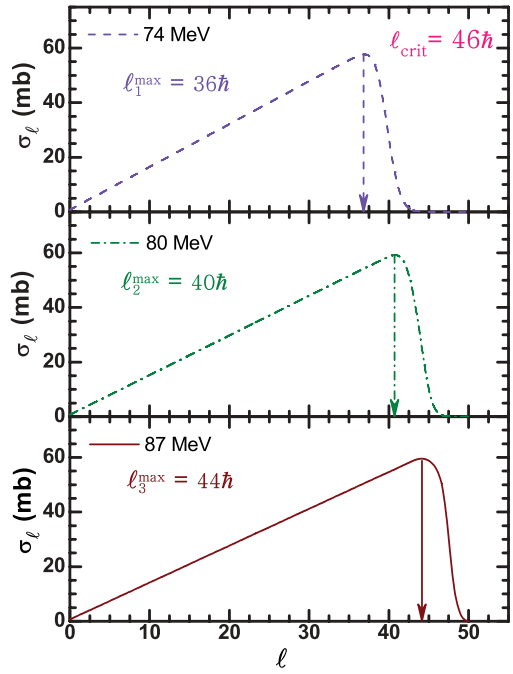

FIG. 6. (Color online) Fusion spin distributions calculated using the code CCFULL [47] for ^{12}C + ^{159}Tb system at $E_{lab} \approx 87$, 84 and 74 MeV, where ℓ is in units of $\hbar$. The value of ℓ_{crit} for fusion calculated using the formulation of Ref. [18].

critical angular momentum for complete fusion (ℓ_{crit}). It is evident from this figure that even at the highest energy studied in the present work, the population of ℓ values are less than the ℓ_{crit} for fusion. As such, the ICF contribution is less probable at these energies as per the SUMRULE model assumptions. However, the present FRRD measurements clearly reveal the significant ICF contribution at these energies, and hence it suggests that a significant number of ℓ waves below ℓ_{crit} may contribute to ICF. The present findings clearly suggest a broad diffused boundary that may penetrate close to the barrier.

IV. CONCLUSION

The recoil range distributions of a large number of radionuclides viz; ^{168}Lu $(3n)$, ^{167}Lu $(4n)$, ^{165}Lu $(6n)$, ^{167}Yb $(p3n)$, ^{165}Tm $(\alpha 2n)$, ^{163}Tm $(\alpha 4n)$, ^{161}Ho $(2\alpha 2n)$, ^{160}Ho^g $(2\alpha 3n)$, and ^{160}Ho^m $(2\alpha 3n)$ populated in ^{12}C + ^{159}Tb interactions at three above-barrier energies have been measured. The analysis of the measured FRRDs of reaction products presented strongly reveals a significant contribution from the partial LMT of the projectile associated with ICF in several α-emitting channels. Different partial LMT components are attributed to the fusion of ^{8}Be and α from the ^{12}C projectile to the target nucleus. The percentage ICF contributions are found to have onset from $\approx$12% above CB. It has been found, in general, that the residues are populated not only via CF but ICF is also found to play an important role in the production of different reaction products involving direct α-cluster emission. The present results have also been compared with literature results, and it may be concluded that instead of Morgenstern's mass-asymmetry

systematics the projectile structure along with α-Q value is also important at the energy range of interest. On the other hand, the SUMRULE model calculations highly underestimate the ICF cross section, which may be due to the assumption that a substantial contribution to ICF comes from the collision trajectories with $\ell > \ell_{\rm crit}$. However, in the energy range of the present study, $\ell_{\rm max} < \ell_{\rm crit}$, thus, significant cross sections for ICF at these beam energies indicate the contribution from collision trajectories with $\ell < \ell_{\rm crit}$. The results obtained from the FRRDs give valuable information for establishing the CF and ICF yields at relatively low bombarding energies and also indicate that the ℓ values lower than $\ell_{\rm crit}$ significantly contribute to the ICF reactions. More data on such reactions is needed to explore the above aspects, so that the assumptions of the SUMRULE model for energies near the barrier, where $\ell < \ell_{\rm crit}$, may be improved upon to explain the experimental data.

ACKNOWLEDGMENTS

The authors thank the Director of the Inter University Accelerator Centre, New Delhi, India, and the Chairman of the Department of Physics, Aligarh Muslim University, for providing all the necessary facilities to carry out the experiment and analysis. We thank Dr. R. K. Bhowmik, R. P. Singh, and S. Muralithar for scientific discussions and support during the experiments. B.P.S. and R.P. also thank the University Grant Commission (UGC) for financial support. A.Y. thanks the UGC of the Government of India for support by the Senior Research program.

[1] E. Holub, D. Hilscher, G. Ingold, U. Jahnke, H. Orf, and H. Rossner, Phys. Rev. C **28**, 252 (1983); **33**, 143 (1986).
[2] M. Cavinato *et al.*, Phys. Rev. C **52**, 2577 (1995).
[3] P. Vergani *et al.*, Phys. Rev. C **48**, 1815 (1993).
[4] D. J. Parker, J. J. Hogan, and J. Asher, Phys. Rev. C **35**, 161 (1987); D. J. Parker, J. Asher, T. W. Conlon, and I. Naqib, *ibid.* **30**, 143 (1984).
[5] S. Sodaye *et al.*, Eur. Phys. J. A **14**, 371 (2002).
[6] N. Added *et al.*, Nucl. Phys. A **540**, 328 (1992).
[7] H. W. Wilschut *et al.*, Phys. Lett. B **138**, 43 (1984).
[8] R. I. Badren, D. J. Parker, and N. Naquib, Eur. Phys. Rev. J. A **12**, 317 (2001).
[9] P. P. Singh *et al.*, J. Phys. Conf. Series **282**, 012019 (2011); EPJ Web Conf. **2**, 10004 (2010).
[10] M. K. Sharma *et al.*, Phys. Rev. C **70**, 044606 (2004); Nucl. Phys. A **776**, 83 (2006); M. K. Sharma, Unnati, D. P. Singh, P. P. Singh, B. P. Singh, R. Prasad, and H. D. Bhardwaj, Phys. Rev. C **75**, 064608 (2007).
[11] B. S. Tomar, A. Goswami, A. V. R. Reddy, S. K. Das, P. P. Burte, S. B. Manohar, and B. John, Phys. Rev. C **49**, 941 (1994); B. S. Tomar, A. Goswami, G. K. Gubbi, A. V. R. Reddy, S. B. Manohar, B. John, and S. K. Kataria, *ibid.* **58**, 3478 (1998).
[12] B. B. Kumar, S. Mukherjee, S. Chakrabarty, B. S. Tomar, A. Goswami, and S. B. Manohar, Phys. Rev. C **57**, 743 (1998).
[13] P. P. Singh *et al.*, Phys. Rev. C **80**, 064603 (2009); **78**, 017602 (2008); Eur. Phys. J. A **34**, 29 (2007).
[14] P. P. Singh, *et al.*, Phys. Rev. C **77**, 014607 (2008), and the references therein.
[15] P. P. Singh *et al.*, Euro. Phys. J. A **34**, 29 (2007).
[16] D. P. Singh *et al.*, Phys. Rev. C **81**, 054607 (2010).
[17] T. Inamura *et al.*, Phys. Lett. B **68**, 51 (1977); **84**, 71 (1979).
[18] J. Wilczynski *et al.*, Phys. Rev. Lett. **45**, 606 (1980).
[19] C. Gerschel, Nucl. Phys. A **387**, 297 (1982).
[20] W. Trautmann, O. Hansen, H. Tricoire, W. Hering, R. Ritzka, and W. Trombik, Phys. Rev. Lett. **53**, 1630 (1984).
[21] I. Tserruya *et al.*, Phys. Rev. Lett. **60**, 14 (1988).
[22] J. Wilczynski *et al.*, Nucl. Phys. A **373**, 109 (1982).
[23] K. Siwek-Wilczynska, E. H. du Marchievan Voorthuysen, J. vanPopta, R. H. Siemssen, and J. Wilczynski, Phys. Rev. Lett. **42**, 1599 (1979).
[24] H. Morgenstern *et al.*, Phys. Lett. B **113**, 463 (1982); **52**, 1104 (1984).
[25] P. P. Singh *et al.*, Phys. Lett. B **671**, 20 (2009).
[26] T. Udagawa and T. Tamura, Phys. Rev. Lett. **45**, 1311 (1980).
[27] J. R. Wu and I. Y. Lee, Phys. Rev. Lett. **45**, 8 (1980).
[28] R. Weiner *et al.*, Nucl. Phys. A **286**, 282 (1977).
[29] J. P. Bondrof *et al.*, Nucl. Phys. A **333**, 285 (1980).
[30] M. Blann, Phys. Rev. C **23**, 205 (1981); Nucl. Phys. A **235**, 211 (1974); Ann. Nucl. Sci. **25**, 123 (1975).
[31] T. Otsuka *et al.*, Phys. Lett. B **121**, 106 (1983).
[32] U. Gupta *et al.*, Nucl. Phys. A **811**, 77 (2008).
[33] U. Gupta *et al.*, Phys. Rev. C **80**, 024613 (2009).
[34] D. P. Singh *et al.*, Phys. Rev. C **80**, 014601 (2009).
[35] A. Yadav *et al.*, Phys. Rev. C **85**, 034614 (2012).
[36] A. Yadav *et al.*, EPJ Web Conf. **17**, 16019 (2011).
[37] A. Yadav *et al.*, EPJ Web Conf. **21**, 08005 (2012).
[38] CANDLE, *Collection and Analysis of Nuclear Data using Linux Network*, B. P. Ajith Kumar *et al.* (DAE **SNP**, Kolkotta, 2001).
[39] E. Browne and R. B. Firestone, *Table of Radioactive Isotopes* (Wiley, New York, 1986).
[40] R. B. Firestone and V. S. Shirley, *Table of Isotopes*, 8th ed. (Wiley, New York, 1996).
[41] SRIM, The Stopping and Range of Ions in Matter code: [http://www.srim.org/SRIM/SRIMLEGL.htm].
[42] Tarasov and Bazin, Nucl. Instrum. Methods Phys. Res. B **204**, 174 (2003); [http://lise.nscl.msu.edu/pace4.html#introduction].
[43] A. Gavron, Phys. Rev. C **21**, 230 (1980).
[44] R. Bass, Nucl. Phys. A **231**, 45 (1974).
[45] F. D. Becchetti and G. W. Greenlees, Phys. Rev. **182**, 1190 (1969).
[46] P. M. Endt, At. Data Nucl. Data Tables **26**, 47 (1981).
[47] K. Hagino *et al.*, Comput. Phys. Commun. **123**, 143 (1999).